3

Fundamentals of Laser Ablation of the Materials Used in Microfluiducs

Tai-Chang Chen and Robert Bruce Darling
University of Washington, USA

1. Introduction

Microfluidics falls into an intermediate range within the spectrum of applications for microfabrication techniques. The width and depth of most microfluidic channels fall in the range of 10-1000 μm, and this feature size is thus small for conventional machine tool microfabrication, but quite large for photolithographically defined etching processes of the type used within the microelectronics industry. In addition, most microfluidic channels occupy only ~10% or less of the surface area of a microfluidic device. Wet chemical or plasma etching processes to produce microfluidic devices therefore take considerable time to complete, based upon the comparatively deep depths that are required for the channels. A comparatively fast wet or dry etching rate of 1 μm/min would still require up to several hours per wafer to achieve these depths. The small surface areas that are etched within this time make conventional batch processing of wafers less attractive economically. In many cases, photolithographically defined microfluidic features with micron scale accuracy are more precise than what is required for these applications.

At high volumes, other microfabrication processes become more applicable for the manufacture of microfluidics. Roll-to-roll stamping, lamination, hot embossing, and injection molding of plastic components offer excellent accuracy, repeatability, and cost effectiveness once the non-recoverable engineering (NRE) costs of molds, dies, and master templates have been paid for. However, the cost of these NRE items is comparatively high, and in most circumstances, production volumes of >1 million parts are required to recover this cost.

For part volumes from 1 to 1 million, laser microfabrication offers an excellent balance between speed, cost, and accuracy for microfluidics. Laser micromachining is also unmatched in the breadth of different of materials that it can process. A single laser system can micromachine materials all the way from lightweight plastics and elastomers up through hard, durable metals and ceramics. This versatility makes laser micromaching extremely attractive for prototyping and development, as well as for small to medium run manufacturing.

The most common criticism of laser micromachining is that it is a serial, rather than batch process, and it is therefore too slow to be economical for high volume manufacturing. While certainly true in some instances, as a generalization, this is not always the case. The processing time per part is the sum of the beam exposure time plus the beam positioning time. For parts which require only minimal volumes of material to be removed, serial

processes such as laser micromachining can indeed be extremely efficient and cost effective. Whereas older laser micromachining systems were often limited by clumsy beam positioning, modern systems incorporate high speed beam positioning and parts handling so that the overall processing time is limited more by the net beam exposure time, which for many applications can be fairly small. A good counter-example to the criticism of serial processing is chip resistor trimming, which is used for almost all 1% tolerance and better metal film chip resistors in the microelectronics industry today and which are produced in extremely high volumes, >10 billion/year.

Microfluidics is becoming increasingly used for miniaturized chemical analysis systems, such as the new generations of lab-on-a-chip applications which are rapidly being developed. The fundamental structure used in microfluidics is the flow channel, but integrated microfluidic systems also incorporate vias, T-junctions, sample wells, reaction chambers, mixers, and manifolds, along with some moving mechanical components such as valves, pumps, and injectors, and often some optical and electrical components for integrated control and sensing. Unlike wet and dry etching which must be carefully formulated to achieve the required material selectivity, laser micromachining can be used to process many different materials and structures at a time. For example, a laser can be used to cut a channel to one depth, cut a via to another depth, trim a metal trace, release a check valve structure, and weld two mating elements together all within the same mounting of the part. This illustrates one of the advantages that serial processing has over traditional batch processing of wafers. Another obvious advantage of serial laser processing is that no masking is required, greatly reducing the time and expense for design changes. Different parts can also be individually customized with virtually no extra tooling overhead. Microfluidics and laser micromachining are an excellent marriage of technologies which will prove essential for the rapid development of these applications.

This chapter will discuss the fundamentals of laser ablation in the microfabrication of microfluidic materials. After briefly describing the various types of lasers which are used for this purpose, the fundamental mechanisms of laser micromachining will be described, along with some data illustrating the performance of some state-of-the-art laser micromachining systems.

1.1 Lasers for micromachining

By far the most common laser used for industrial processing is the carbon dioxide (CO_2) gas laser. This popularity comes from its unique combination of high average power, high efficiency, and rugged construction. Unlike the original glass tube style gas lasers, the modern CO_2 lasers which are used for materials processing are of a hard sealed waveguide construction that use extruded aluminum RF driven electrodes to excite a $CO_2/N_2/He$ gas mixture. The lasing transitions are from asymmetric to symmetric stretch modes at 10.6 μm, or from asymmetric stretch to bending modes at 9.4 μm of the CO_2 molecule (Verdeyen, 1989). Within each of these vibrational modes there exist numerous rotational modes, and hundreds of lasing transitions can be supported by excitation into the parent asymmetrical stretch mode of the CO_2 molecules. This large number of simultaneous lasing modes along with the efficient excitation coupling through the N_2 gas is what allows CO_2 lasers to achieve power levels up to 1 kW with electrical to optical conversion efficiencies of nearly 10%. CO_2 lasers emit in the mid-infrared (MIR), most commonly at 10.6 μm, and they principally interact with their target materials via focused, radiant heating. They are used

extensively for marking, engraving, drilling, cutting, welding, annealing, and heat treating an enormous variety of industrial materials (Berrie & Birkett, 1980; Crane & Brown, 1981; Crane, 1982). For micromachining applications, the long wavelength translates into a fairly large spot diameter of ~50-150 μm with a corresponding kerf width when used for through cutting.

The most common solid-state laser used in industry is the neodymium-doped yttrium-aluminum-garnet, or Nd:YAG. The YAG crystal is a host for Nd^{3+} ions, whose lasing transitions from the excited $^4F_{3/2}$ band to the energetically lower $^4I_{11/2}$ band produces emission at 1.064 μm in the near-infrared (NIR) (Koechner, 1988; Kuhn, 1998). Nearly all industrial Nd:YAG lasers are now pumped by semiconductor diode lasers, usually made of GaAlAs quantum wells and tuned to emit at ~810 nm, for optimum matching to the pertinent absorption band of Nd:YAG. Semiconductor diode pumping of Nd:YAG offers much more efficient pumping with minimal energy being lost to heat, since the diode emits only into that part of the spectrum which is needed for the pumping. However, semiconductor diode pump lasers can only be made up to ~100 W, and thus these are used only for Nd:YAG lasers of low to moderate average powers. Most industrial Nd:YAG lasers are also Q-switched, usually by means of a KD*P electrooptic intracavity modulator. When the modulator is in the non-transparent state, the pumping of the Nd:YAG rod allows the population inversion to build up to very high levels. When the modulator is rapidly switched to the transparent state, the energy stored in the inverted population is discharged at once into a single giant pulse of narrow duration and high peak power. Typical Q-switched pulse widths are in the range of ~25 ns, and with firing repetition rates of ~40 kHz, the duty cycle of a Q-switched Nd:YAG laser is ~1:1000. A ~10 W average power Nd:YAG laser can then produce pulses with peak powers of ~10 kW. This high peak power makes Q-switched Nd:YAG lasers ideally suited for nonlinear optical frequency multiplication through the use of an external cavity harmonic generating crystal such as KDP, KTP, $LiNbO_3$, or BBO. Most commonly, the 1064 nm output from the Nd:YAG is frequency doubled to produce a green output at 532 nm. The 1064 nm output can also be frequency tripled to produce 355 nm in the near ultraviolet (UVA band), or frequency quadrupled (using a sequential pair of doublers) to 266 nm in the deep ultraviolet (UVC band). All four of these commonly available Nd:YAG output wavelengths are extremely useful for micromachining purposes (Atanasov et al., 2001; Tunna et al., 2001).

Copper vapor lasers have also proven their use in high accuracy micromachining (Knowles, 2000; Lash & Gilgenbach, 1993). Similar to the Nd:YAG, they are Q-switched systems which produce high intensity pulses of typically ~25 ns at rates of 2-50 kHz and average powers of 10-100 W. Unlike the Nd:YAG, they emit directly into the green at 511 nm and 578 nm, and thus do not require a nonlinear crystal for frequency multiplication to reach these more useful wavelengths. Copper vapor lasers also have excellent beam quality and can usually produce a diffraction-limited spot on the substrate with only simple external beam steering optics. The disadvantage of copper vapor lasers is that they tend to have shorter service life and require more maintenance than Nd:YAG lasers. Frequency multiplying crystals have now become a ubiquitous feature of commercial Nd:YAG lasers, and as a result, Nd:YAGs have largely displaced the copper vapor laser for industrial micromachining applications.

Excimer lasers have also found wide use in materials processing applications. Excimer lasers operate from a molecular transition of a rare gas-halogen excited state that is usually pumped by an electric discharge. The XeCl excimer laser, which emits at 308 nm, is prototypical of these in which a pulsed electric discharge ionizes the Xe into a Xe^+ state and

ionizes the Cl_2 into a Cl^- state. These two ions can then bind into a Xe^+Cl^- molecule which will loose energy through a lasing transition as it relaxes back to the XeCl state. The resulting ground state XeCl molecule readily dissociates, and these products are then recycled. Other commonly used excimer lasers are the XeF which emits at 351 nm, the KrF which emits at 249 nm, the ArF which emits at 193 nm, and the diatomic F_2 which emits at 157 nm (Kuhn, 1998). Like other laser systems which are well matched to applications in materials processing, excimer lasers produce pulses of ~50 ns with repetition rates of ~100 Hz to ~10 kHz and average powers of up to a few hundred Watts. Excimer lasers are fairly efficient in their electrical to optical conversion efficiency, but their use of highly reactive halogen gases at high pressures requires significantly more servicing and maintenance than other types. One of the most important properties of excimer lasers is their ability to create a rather large spot size which can be homogenized into a high quality flat top beam profile of up to several cm in dimension. Because of this, they have been the pre-eminent source for coherent UV radiation at moderate power levels, they can be used both as a masked or a scanned exposure source, and currently they are used extensively for UV and deep UV lithography as well as several other applications in thin film recrystallization and annealing. At higher beam intensities, they can be used for surface ablation of materials, and due to the short wavelength and short pulse width, they typically produce clean, crisp features in metals, ceramics, glasses, polymers, and composites, making them adaptable for numerous micromachining applications (Gower, 2000).

Short laser pulses, on the order of a few tens of nanoseconds, are a desirable feature for laser micromachining applications, and these can be produced with many different laser systems. As will be discussed in more detail later, the short pulse width produces nearly adiabatic heating of the substrate which allows the substrate surface temperatures to quickly reach the point of vaporization with minimal heating effects on the surrounding areas. There has been interest in laser systems which can produce even shorter pulse widths, and the foremost candidate for this has been the Ti:sapphire laser. The Ti:sapphire laser has the unique feature of being tunable over a surprisingly large fluorescence band: from ~670 nm to ~1090 nm. For efficient pumping, it needs to be optically excited in its absorption band, which is centered about 500 nm, and for which argon ion lasers and frequency doubled Nd:YAG lasers provide excellent sources (Kuhn 1998). Most Ti:sapphire lasers are configured into an optical ring resonator arrangement with a set of birefringent filters for tuning. In addition, the ring cavity usually contains a Faraday rotator and wave plates to limit the propagation to only one direction around the ring. This arrangement is well suited for wide tuning and also mode locking, through which very short pulses, on the order of a few tens of femtoseconds can be produced. Ti:sapphire lasers have thus become a key resource for spectroscopy and research on ultrafast phenomena. The Ti:sapphire laser is also capable of average powers of up to several Watts, which makes it a viable tool for micromachining. Although its operation is at longer wavelengths than those normally preferred for micromachining, its capability for tuning and producing ultrashort pulses makes it attractive for research in this area. Since it requires a pump laser of ~10 W which is already in the green, and its more complicated optical system requires more maintenance and user savvy, it is presently not a common choice for industrial micromachining applications, but this may change in the future. There are many other new laser systems under development which offer efficient generation of green light at the power levels and pulse widths required for micromachining. It is worthwhile to realize that the field of laser sources is constantly changing.

In general, the lasers best suited for micromachining are those that produce short pulses of high intensity at short wavelengths. Pulse widths of less than a microsecond are needed to allow the formed plasma to extinguish in between pulses so that subsequent pulses are not scattered and absorbed. Time for the debris plume to clear takes longer, often up to tens or hundreds of milliseconds, but its optical attenuation is usually less. Concentrating the laser radiation into short pulses of high intensity also has the benefit of more adiabatic heating of the substrate, bringing its temperature up to the vaporization point before too much of the heat can diffuse vertically and laterally away from the intended ablation zone. Shorter wavelengths generally have higher absorption coefficients in most materials, and they are thus absorbed nearer to the surface where the ablation is intended to occur. Shorter wavelengths can also be focused into a proportionally smaller diffraction-limited spot, which improves both the accuracy and precision of the ablation process. Typical working spot diameters for UV lasers in the 350 nm range are ~25 μm, although this is larger than the theoretical diffraction limit.

2. Fundamental laser micromachining processes

Laser micromachining includes a number of different processes which are differentiated by the feature geometry and the manner in which material is removed from the substrate (Ion, 2005; Schuöcker, 1999). Cutting in this context refers to using the beam to slice all of the way through a thin sheet of substrate material, leaving behind a kerf which extends completely through to the opposite side of the substrate. As is commonly the case in laser cutting of sheet metal, the material removed from the kerf is predominantly ejected out the opposite side. Ablating is usually taken to mean removal of material in a thin layer from one side only, giving only partial penetration into the thickness of the substrate, and the removed material must necessarily be ejected from the same side as which the laser is incident. In both cases, the newly removed material is ejected primarily through the kerf which has just previously been cut and which trails along behind the laser beam as it is moved along the tool path. Whereas cutting and ablating can create geometries of any shape, drilling refers to the creation of a nominally circular hole with minimal lateral translation of the beam, with either through or blind penetration. If the laser beam is held in one fixed position and pulsed, the process often termed percussion drilling, whereas if the beam is swept around in a circular pattern to first roughly remove the bulk material and then completed with a fine finishing pass to accurately define the perimeter, the process is called trepanning. Percussion drilling produces holes whose diameter is roughly the same as the diameter of the laser beam, while trepanning produces holes whose diameter is larger than the beam diameter. Because drilling does not produce a trailing kerf, all removed material must be ejected from the same side as which the laser beam was incident, and drilling is thus necessarily an ablative process, regardless of whether it creates a through or blind hole (Voisey et al., 2003).

The removal of material can involve both thermal and chemical processes, depending upon how the laser radiation interacts with the substrate. At longer wavelengths, the photon energy is insufficient to provide anything more than simple heating of the substrate. At sufficiently high intensities, however, the heating can be concentrated enough to first melt the substrate material within a localized zone, and then vaporize it in those areas where the laser intensity and subsequent heating is higher. The substrate material is thus removed via a transition to the gas phase, although the vaporized material is often subsequently ionized

by the laser radiation, leading to a plasma and plume that can have the effect of occluding the incident beam. It is customary to identify three zones around the incident beam: the heat-affected zone or HAZ, the melt zone, and the vaporization zone. Some materials can pass directly from the solid phase into the vapor phase by sublimation, and for these the melt zone is absent. Both melting followed by vaporization or direct sublimation are purely thermal ablation processes.

At shorter wavelengths, the photon energy may reach the level of the chemical bond strength of the substrate. Laser radiation may then break these chemical bonds through direct photon absorption, leading to volatilization of the substrate into simpler compounds. For most organic polymers, this photolysis process produces mainly H_2O and CO_2. This occurs typically for photon energies above 3.5 eV, or for wavelengths shorter than ~350 nm, i.e. into the near UV part of the spectrum. Because the photon energy is lost to chemical bond scission, the heating effects of the beam are greatly reduced, and this regime is sometimes referred to as "cold laser machining," non-thermal ablation, or photochemical ablation. This greatly reduces the transient thermal stresses that occur as part of thermal ablation, and the result is less bowing, warping, and delamination of the substrate, as well as fewer edge melting effects which degrade feature accuracy (Yung et al., 2002). Since the peak temperature rise is greatly reduced, conductive heat flow away from the irradiation area is also reduced, and better dimensional control of the micromachined structure is obtained. There has been a general trend toward using shorter wavelength lasers for micromachining over the past two decades of development. Currently, UV lasers in the 350 to 250 nm range dominate the industrial market for the above reasons.

Thermal ablation and photochemical ablation are two ideal extremes, and laser micromachining can often involve a combination of both for any given material or composite. In addition, there are several secondary processes which can arise due to the steep temperature gradients which are produced. If the laser beam is composed of short, high-intensity pulses, as would be typical for Q-switched systems, then the adiabatic heating of the substrate can cause sufficiently high temperature gradients for which differential thermal expansion and acoustic shock can produce surface cracking or spalling of the substrate (Zhou et al., 2003). Micron-sized flakes of the substrate can be explosively ejected from this process without requiring the additional thermal energy to fully vaporize the material. This is typically more prevalent for brittle materials with low thermal conductivity, e.g. ceramics and some glasses. For materials which readily oxidize, the rapid cycle of laser heating and cooling of the melt zone can cause the formed oxide film to flake off in chips from the compressive stress that was built into the oxide during the process. This is typically more prevalent for reactive metals such as chromium, nickel, iron, and copper. Thermal spalling and oxide chipping both create debris particles which are significantly larger than the redeposition of fully vaporized substrate material. Because both thermal spalling and oxide chipping occur after the melt zone has refrozen, they leave behind a surface finish which is typically more frosted or matte in visual appearance, and microscopically cusped on a smaller scale.

Inherent to all laser micromachining is the creation of a plume of ejected material, either fully vaporized or sometimes containing micron-sized debris flakes. This plume requires time to disperse, and if the next laser pulse arrives before this takes place, the laser radiation will usually produce some degree of ionization as it is absorbed by the vapor. This ionization of the vaporized material produces a plasma which, in addition to being fairly energetic and reactive, can absorb the laser radiation further, sometimes occluding the path

for the beam to reach the substrate (Eloy, 1987). This luminous plasma is what is usually responsible for the "sparkles" that mark the travel of the laser beam across the substrate. Achieving beam positioning and pulse timing to avoid the plasma and plume occlusion of the beam is a central part of tuning the recipe for any laser micromachining. This problem is generally severe in continuous wave (CW) laser micromachining, but greatly reduced for pulsed lasers which are Q-switched. While the complete plume of vaporized material usually does not have time to fully disperse in between Q-switched pulses, the more optically opaque and higher density plasma does, and laser ablation can continue onward with usually only minor attenuation. If the beam positioning is not well designed, however, the plasma and plume can become trapped into the confined spaces of the kerf, and greater time will be required for their dispersal. The most common symptom of this effect is a reduced depth of ablation for a given beam transversal rate.

2.1 Ablation process models

Laser ablation involves a complex interaction between optical, thermal, and chemical processes, but some simplifications can lead to models which can be useful for characterization, optimization, and troubleshooting of the process. Most such models start with the optics of a Gaussian beam and compute the conductive flow of heat from this source to find the temperature distribution, adding in the thermal effects which are needed to account for melting and vaporization of the substrate (Engin & Kirby, 1996; Kaplan, 1996; Olson & Swope, 1992). An idealized geometry is illustrated in Fig. 1 in which a circularly symmetric Gaussian laser beam is moved across the substrate at a constant speed v in the $+x$ direction. The beam has an average power of $P_0 = \pi r_B^2 I_0$, where I_0 is the peak intensity and r_B is the *1/e* beam radius. The beam propagates in the $+z$ direction and meets the substrate surface in the x-y plane. The situation is more easily described by using the relative coordinate $\xi = x - vt$ which moves along with the laser beam.

The interaction of the laser beam with the substrate first involves absorption of the optical radiation and its conversion into heat for thermal (non-photo-chemical) ablation. Shorter wavelengths are absorbed more strongly at the surface with a higher absorption coefficient α, and since this is usually ~10^4 cm^{-1} or greater, the heating is effectively concentrated at the surface of the substrate. Volumetric heating effects have been considered by Zhang, et al. (2006). The surface heating density is then

$$q(\xi, y) = (1 - R) I_0 \exp\left(-\frac{\xi^2 + y^2}{r_B^2} \right) \qquad [W / m^2],$$

where R is the reflectivity loss from the surface of the substrate.

The heat transfer within the substrate is entirely by conduction, so the resulting temperature field is given by a solution to the heat conduction equation (Carslaw & Jaeger, 1959)

$$\frac{\partial T}{\partial t} - D\nabla^2 T = 0,$$

where $D = \kappa/\rho C$ is the thermal diffusivity, κ is the thermal conductivity, ρ is the mass density, and C is the specific heat capacity. The surface heating density provides a source boundary condition for the solution of the heat conduction equation. Ashby and Easterling (1984) have shown that a close analytical approximation to the solution of this problem is given by

$$T(\xi = 0, y, z, t) - T_0 = \frac{(1-R)P_0}{2\pi\kappa v\left[t(t + r_B^2 / D)\right]^{1/2}} exp\left(-\frac{(z+z_0)^2}{4Dt} - \frac{y^2}{4Dt + r_B^2}\right),$$

where T_0 is the initial temperature of the substrate, and z_0 is a parameter chosen to eliminate the surface singularity as $t \rightarrow 0$.

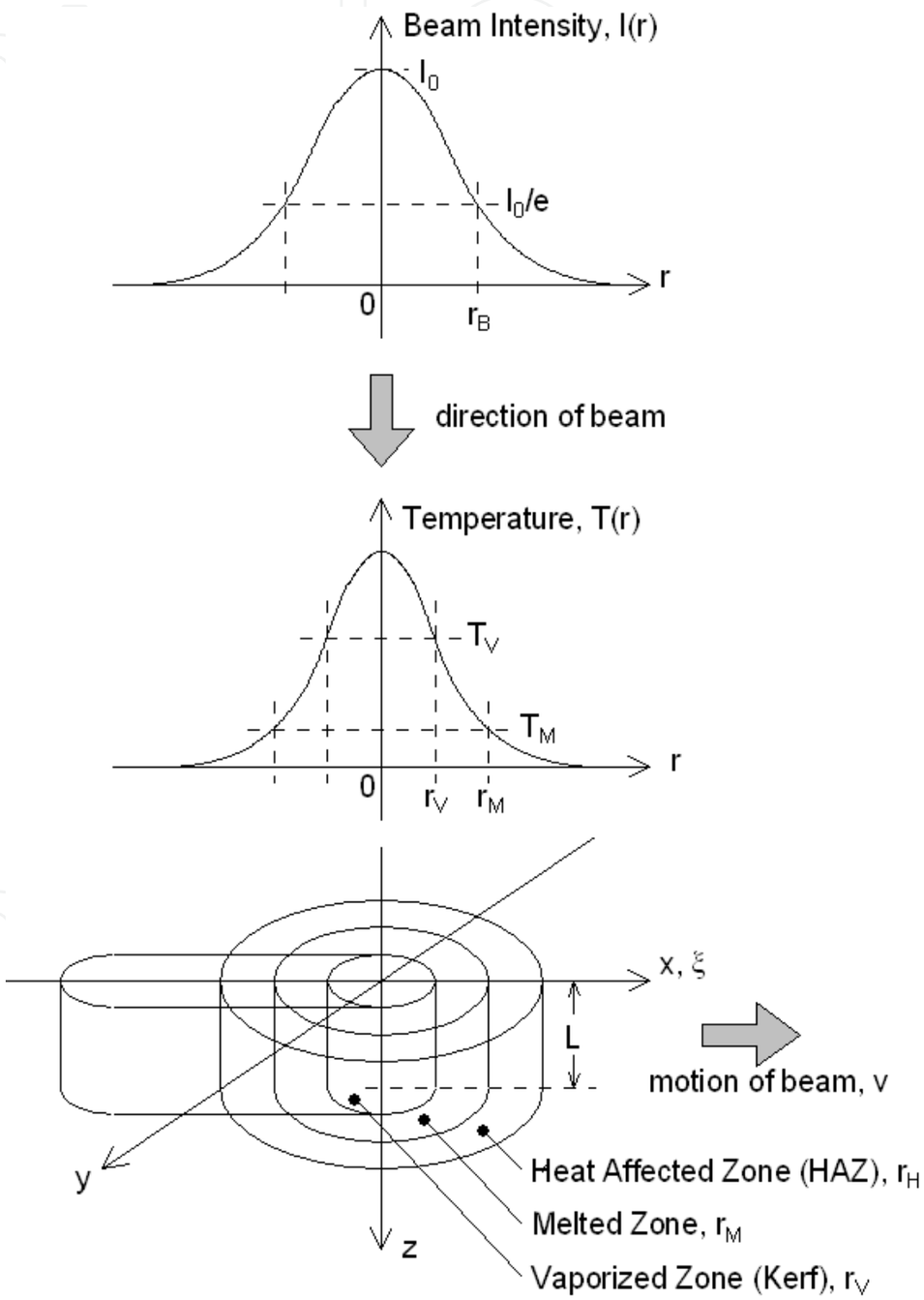

Fig. 1. Geometry and intensity and temperature profiles for laser ablation.

With a sufficiently large laser average power P_0 and a sufficiently slow beam traversal rate v, the resulting temperature field can produce first melting and then vaporization of the substrate. Three zones are commonly defined based upon the phase changes: a heat affected zone or HAZ with a radius r_H, a melted zone with a radius r_M, and a vaporized zone with a radius r_V, which forms the final kerf of width $2r_V$. For simplicity, the depth of cut is taken to be L for all three of these zones, as shown in Fig. 1. These radii are defined by the points at which the peak temperature equals the melting point T_M or the vaporization point T_V for the substrate material. It is important to recognize that these three radii are dependent upon the beam radius r_B, but are not equal to it. Similarly, the radial temperature distribution is not the same as the incident Gaussian beam shape.

In addition to simply raising the temperature of the substrate material, the incident laser power must also be used to change the phase of the material, first from solid to liquid, and then from liquid to vapor, in the case of simple thermal ablation. This energy balance is an important aspect of the ablation process model, and it can be described by the following conservation of energy relation,

$$(1-R)P_0 = \frac{2\pi\kappa L(T_M - T_0)}{\ln(r_H / r_M)} + 2(r_M - r_V)LvE_M + \rho C(r_M - r_V)Lv(T_V - T_M) + 2r_V LvE_V ,$$

where $(1 - R)P_0$ is the optical power that is absorbed by the substrate, v is the beam traversal speed, and L is the depth of the cut. The first term on the right hand side is the power required to bring the temperature of the substrate up to the melting point T_M at the inner boundary of the HAZ. The thermal conductivity is $\kappa = \rho CD$. Within the melted zone, $r_M < r < r_V$, additional power must be added for the melting phase transition, as well as to raise the temperature up to the vaporization point T_V at the inner boundary of the melted zone. The rate at which the beam sweeps out new material volume to melt is $2(r_M - r_V)Lv$ [m^3/s], and the latent heat of melting is E_M [J/m^3], which together give the second term. The third term on the right hand side is the power required to support the temperature difference of $T_V - T_M$ across the melted zone. Similarly, the fourth term on the right hand side is the additional power required to vaporize the material in the kerf, where E_V is the latent heat of vaporization [J/m^3]. The latent heats of melting and vaporization are effectively constants which subtract from the applied optical power that falls within the melted and vaporized zones.

Most notable in the energy balance equation is the direct tradeoff that exists in the last three terms between the depth of cut L and beam traversal speed v. This makes the assumption that the incident beam does not become occluded by the features or debris that the ablation process creates. For CW laser cutting the debris plume and plasma can significantly attenuate the beam, leading to a reduction in the optical power that is available for subsequent ablation. Q-switched lasers with nanosecond pulses suffer far less from this problem, since the time between laser pulses allows the plasma time to extinguish (Chang & Warner, 1996). The above energy balance equation works fairly well for cutting depths L of up to a few beam diameters (Yuan & Das, 2007), but when the aspect ratio of the kerf becomes extreme, $L >> 2r_V$, the sidewalls of the kerf will lead to beam reflections and scattering, and the change in depth may take the beam interaction beyond its depth of focus, both of which will have the effect of reducing the available intensity and slowing down the vertical ablation rate for deeper cuts (Bang et al., 1993). The concave bottom of laser drilled holes may also defocus the beam (Vatsya et al.,2003; Zhang ei al.,2008). This basic model has

been extended to include the effects present in trepanning of holes (Zeng et al., 2005), and for trepanning with annular beam profiles (Zeng et al., 2006).
Laser ablation departs somewhat from the above model when the process involves a photochemical component. In this case, a significant fraction of the photons are absorbed directly for the process of breaking chemical bonds in the substrate, and these photons do not produce direct substrate heating, as would be the case for pure thermal ablation. Process models for this situation must break the photon flux into a thermally absorbed portion and a photochemical portion. The thermal portion behaves as per the above model description, while the photochemical portion creates volatilized products in proportion to the energy density of the specific bonds which are broken. Simple energy balance arguments are useful for predicting the photochemical ablation rate, under the assumption that any left-over energy that does not directly produce photochemical ablation is directed toward substrate heating of the same region. The relative split of the incident photon flux between thermal and photochemical ablation is usually taken to be proportional to the relative absorption coefficients of the two processes. However, it must be cautioned that the appropriate absorption coefficients are themselves temperature dependent and proper modeling of the optical absorption becomes a central problem in any multi-physics simulation of ablation.

2.2 Optical absorption

The most important principle of laser micromachining is that the laser output wavelength must be one which is strongly absorbed by the material to be processed. If the material is highly transparent at the wavelength of the laser, then no optical absorption and energy transfer will take place. For semiconductors and other crystalline materials, this normally means that the photon energy must be greater than the energy bandgap. For polymers and other amorphous materials, the photon energy must be greater than the energy difference between the lowest unoccupied molecular orbital (LUMO) and the highest occupied molecular orbital (HOMO). For both of these cases, that usually entails a laser emitting in the visible or UV with photon energies of ~1 eV or greater.

2.2.1 Absorption of laser radiation

The primary interaction between laser radiation and a solid is photochemical excitation of electrons from their equilibrium states to some excited states by the absorption of photons. Some of these transitions are schematically shown in Fig. 2. Interband transitions take place when photon energy is larger than bandgap of the material. In this process, electron-hole pairs are generated. The free electrons may jump back from conduction band to valence band through thermal (dashed lines) or photochemical processes. If the photon energy is less than bandgap of the material, the energy can be absorbed by defect levels in the banbgap or produce Intraband transitions. Both transitions will induce thermal processes as electrons jump back to valence band. With higher laser light intensities, multi-photon absorption is favored, because the probability of non-linear absorption increases strongly with laser intensity. The coherent multi-photon transitions would generate electron-hole pairs similar to interband transitions. (Linde et al., 1997)
Thus, the initial electronic excitation is followed by complex secondary processes, which can be classified into thermal and photochemical processes. The type of interaction between laser radiation and the material depends on laser parameters (wavelength, pulse duration, and fluence) and on the properties of the materials (Baeuerle, 2000; Mai & Nguyen, 2002).

Laser ablation (material removal) can be analyzed on the basis of photothermal (purely pyrolytic), photochemical (purely photolytic), and photophysical processes, in which both thermal and non-thermal mechanisms contribute to the overall ablation rate.

2.3 Thermal process

The thermal transition of the electrons can be described by the relaxation time τ_T as shown in Fig. 2. When τ_T is smaller than the time required for desorption of species from the surface, τ_R, a photothermal process occurs. Thus, the photothermal ablation is based on the excitation energy being instantaneously transformed into heat. Due to the rapid dissipation of the excitation and ionization energy from the electrons to the lattice, the material surface is heated rapidly and vaporized explosively with or without surface melting. This regime applies to pulsed laser ablation by infrared- (IR-) and visible- (VIS-) laser radiation, and to most cases of ultraviolet- (UV-) laser radiation with nanosecond and longer pulses. These result in relatively high ablation rates and a rough surface finish (Baeuerle, 2000; Ehlich & Tsao, 1989; Luft et al., 1996; Schubart & Otto, 1997).

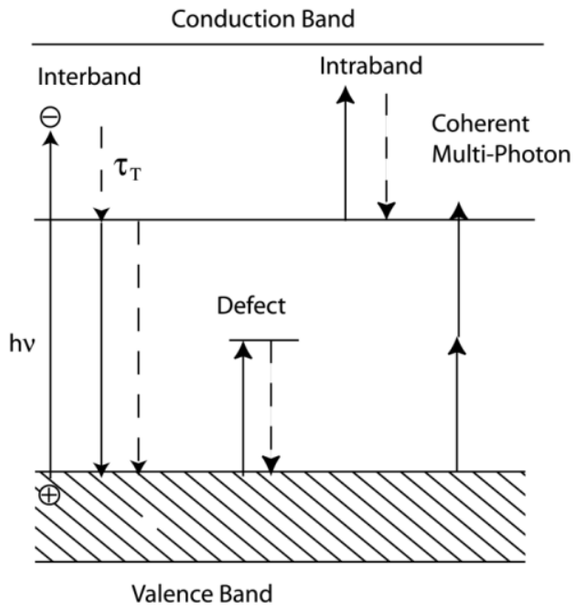

Fig. 2. Schematic of different types of electronic excitation in a solid.

With moderate-to-high laser fluences, and pulse lengths of nanoseconds, screening of the incident radiation by the vapor and plasma plume becomes important. Screening of the incident laser light by absorption and scattering within the vapor plume diminishes the intensity that reaches the substrate. The ablation rate depends on photon energy, laser fluence, spot size and material properties and is in a range between 0.1 and several μm/pulse to be considered as a useful machining method. Additionally, with shorter wavelengths of laser radiation, the laser-plasma interaction becomes less pronounced (Baeuerle, 2000).

2.4 Photochemical process

If $\tau_T >> \tau_R$, the laser excitation can result in direct bond scission, the electrons freed from the broken bonds will be desorbed from the surface, and the process will be photochemical in

nature. With purely photochemical (non-thermal) processes, the temperature of the system remains essentially unchanged under laser irradiation. The ablation rate is relatively slow (≤ 1μm/pulse), but high surface quality can be achieved because of the absence of surface melting and explosive evaporation of the material (Baeuerle, 2000; Mai & Nguyen, 2002).

3. Nd: YAG 266 nm and 355 nm laser micromachining

3.1 Laser ablation settings

Chen and Darling (2005, 2008) have reported sysmatic studies of laser micromachining using Nd:YAG 266 nm and 355 nm lasers recently. An Electro-Scientific Industries (ESI) model 4440 laser micromachining system with a Light Wave Enterprises 210 diode-pumped frequency-tripled (355 nm) and a Photonics Industries diode-pumped frequency-quadrupled (266 nm) Nd:YAG laser were used to micromachine the samples. Output powers of the 355 nm laser were 4.8 W at repetition rate of 10 kHz and 3.0 W at repetition rate of 20 kHz, and that of the 266 nm laser was 0.5 W at repetition rate of 5 kHz. The stage was moved up and down to adjust the z-axis to focus and de-focus the laser beam on the samples. The x-y stage allowed scan speeds from 0 to 250 mm/s. The laser scan speed and repetition rate were adjusted to control the total energy of micromachining, and the focus/defocus was adjusted by moving z-axis stage up to control the laser fluences of the laser spots as shown in Table 1.

The microfluidic materials, such as sapphire, silicon and Pyrex, were micromachined by both 266 nm and 355 nm Nd:YAG lasers. A series of 1 mm × 1 mm square cavities were created by laser micromachining with various laser machining conditions. Fig. 3 and Fig. 4 depict the typical laser micromachining cavities of sapphire and silicon. The ablation square cavities were inspected by an SEM and were measured for depth using an optical microscope and a scanning profilometer. Fig. 5 shows typical measurement data using a Tencor/KLA P-15 profilometer. A certain amount of solidified molten silicon remains in the ablation area after laser machining (Dauer et al., 1999). Thus, silicon wafers were cleaned and etched using a 22 wt% KOH solution at 75°C for 4 minutes to clear the ablation debris.

Z-position[a] (μm)	Fluence[b]		
Repetition Rate (Hz)	10k (355 nm)	20k (355 nm)	5k (266 nm)
0	866	271	50.93
300	96.24	30.01	24.02
600	34.65	10.83	13.93
900	17.68	5.52	9.08
1200	10.69	3.34	6.39
1500	7.16	2.24	4.73
1800	5.13	1.60	3.65
2100	3.85	1.20	2.90

[a]Laser focus at 0 z position, the z position shows the distance of the stage moving up;
[b]Laser fluence was calculated by energy per pulse/ spot size area; fluence unit = J/cm^2

Table 1. The fluences of the laser versus z-stage positions

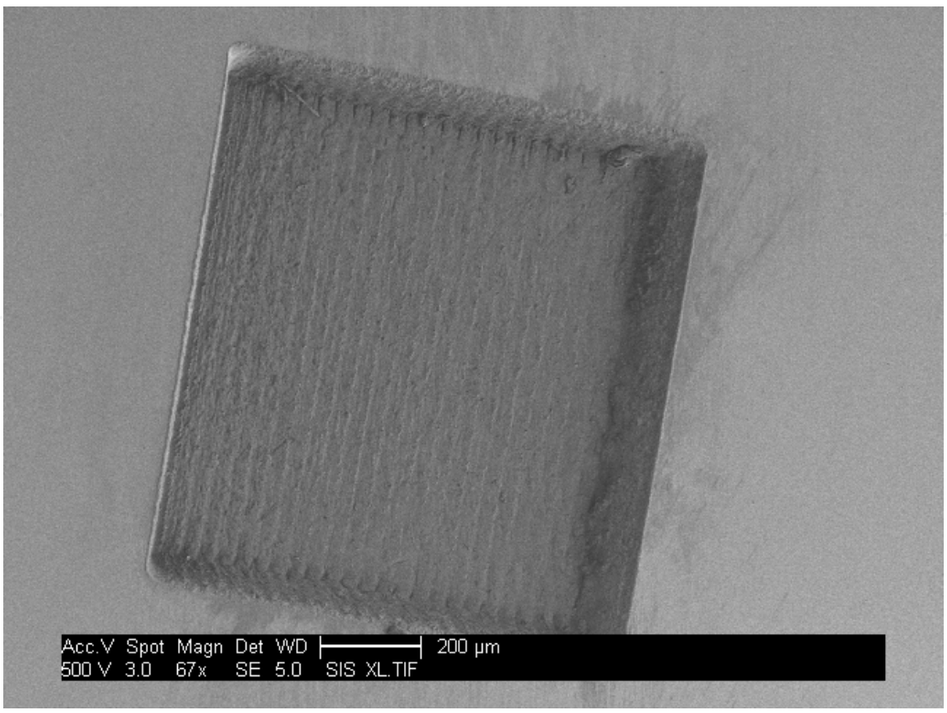

Fig. 3. The SEM image of Nd:YAG laser micromachining on sapphire

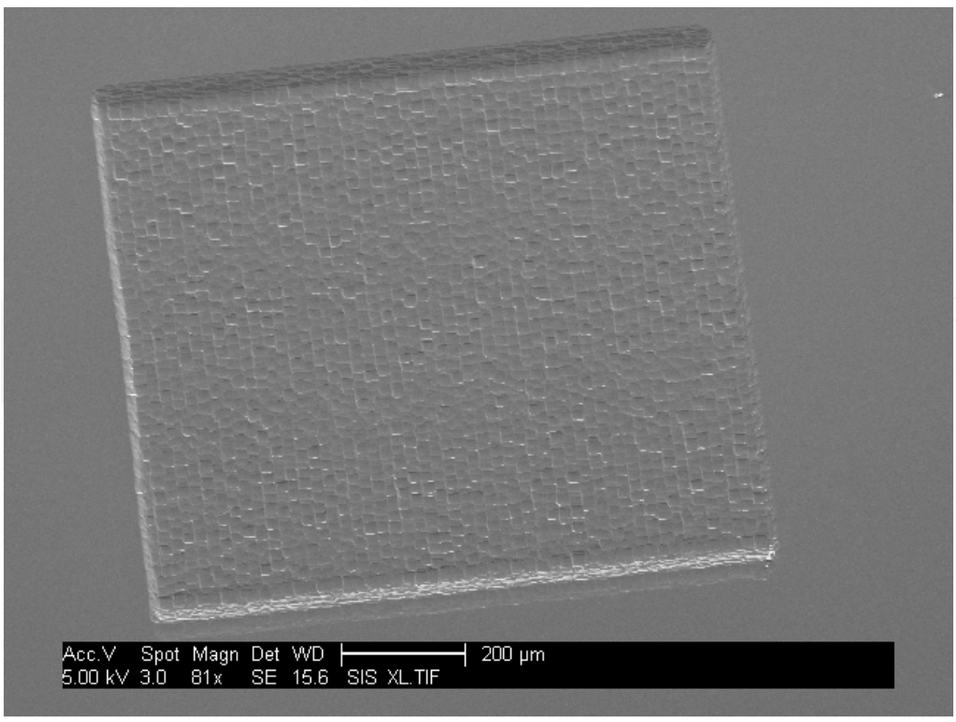

Fig. 4. SEM image of Nd:YAG laser micromachining on silicon.

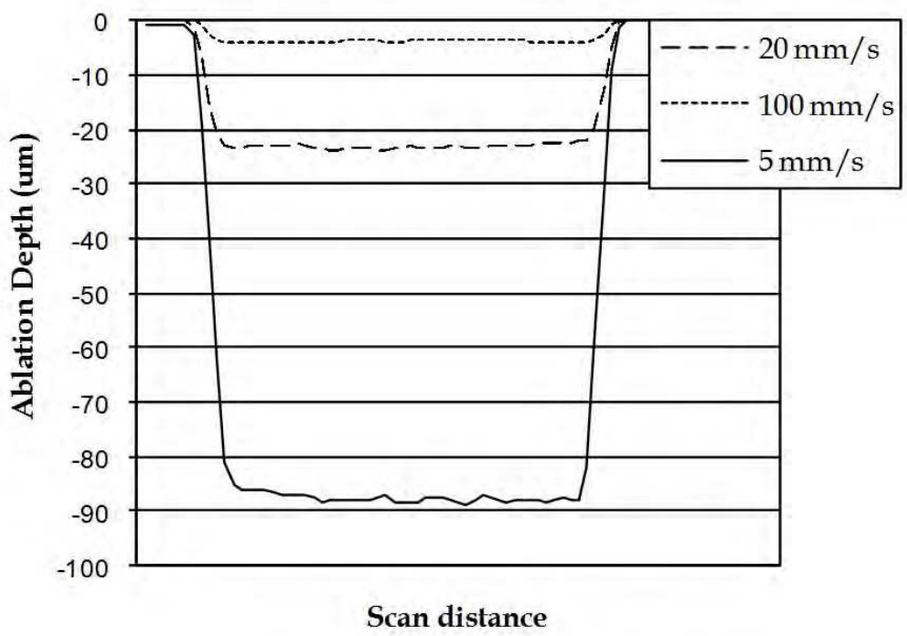

Fig. 5. Depth profiles for 355 nm Nd:YAG laser micromachining of sapphire with fluence of 9.27 J/cm^2 and virious scan speeds.

3.2 Laser micromachining ablation rate

The ablation rates of the laser micromachining were calculated as:

$$\frac{\text{Total removed volume of the material}}{\text{The number of total pulses} \times \text{spot size area}}$$

Figures 6 - 8 show the plots of ablation rates as a function of laser fluences with various laser scan speeds for sapphire, silicon and Pyrex using both Nd:YAG 266 nm and 355 nm lasers. It is observed that in the cases of both sapphire and Pyrex, the 266 nm laser provides higher ablation rates than the 355 nm laser under the same micromachining conditions. On the other hand, Fig. 7 (silicon) shows the varied ablation rates of Nd:YAG 355 nm laser micromachining using 20 mm/s and 50 mm/s scan speeds. The varied result is caused by the plume screening effect on the slower scan speed laser micromachining condition . In this case, the dwell time of laser light on the surface of the silicon is longer than the time for vapor/plasma formation, which attenuates the intensity of incident laser radiation.

The threshold fluences of laser micromachining of sapphire and silicon were calculated as shown in Table 2. All samples either did not exhibit fixed laser ablation threshold values or showed surface melting phenomena. Those results indicate that a thermal process was engaged in the laser micromachining of all the materials micromachined by both 266 nm and 355 nm Nd:YAG lasers. In general, the ablation rates using Nd:YAG 266 nm laser are higher than using 355 nm laser. This is due to the 266 nm laser producing a greater photochemical component.

		Sapphire		Silicon	
	Scan speeds	5 mm/s	10 mm/s	20 mm/s	50 mm/s
Threshold Fluence J/cm²	266nm Nd:YAG	0.4	0.4	0.96	0.95
	355nm Nd:YAG	1.19	1.10	1.31	1.29

Table 2. The threshold fluences of laser micromachining of sapphire and silicon

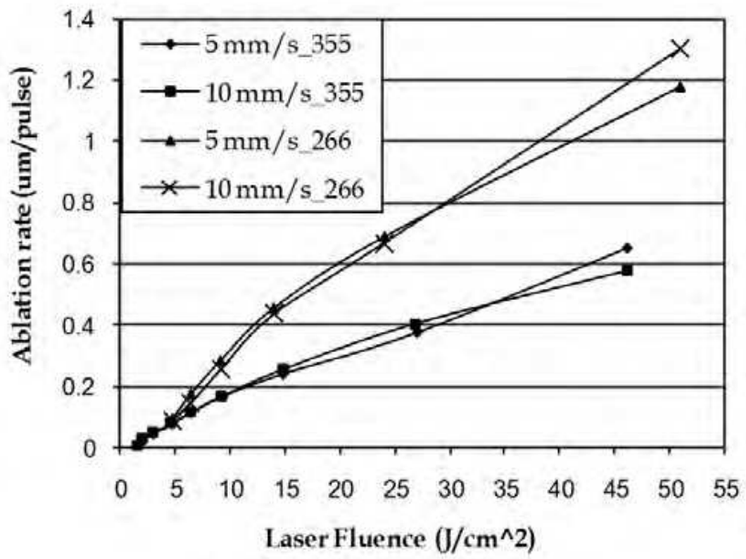

Fig. 6. The ablation rates for laser micromachining versus laser fluence for sapphire with different cutting speeds using 266 nm and 355 nm Nd:YAG lasers.

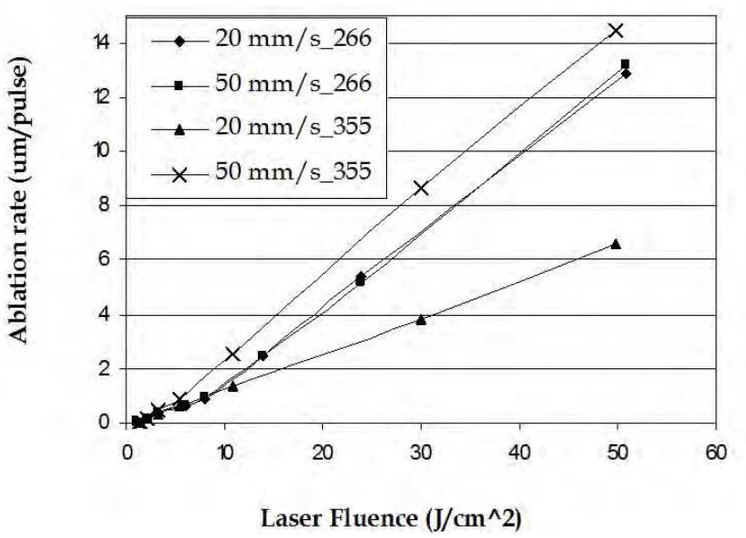

Fig. 7. The ablation rates of laser micromachining versus laser fluences for silicon with different cutting speeds using 266 nm and 355 nm Nd:YAG lasers.

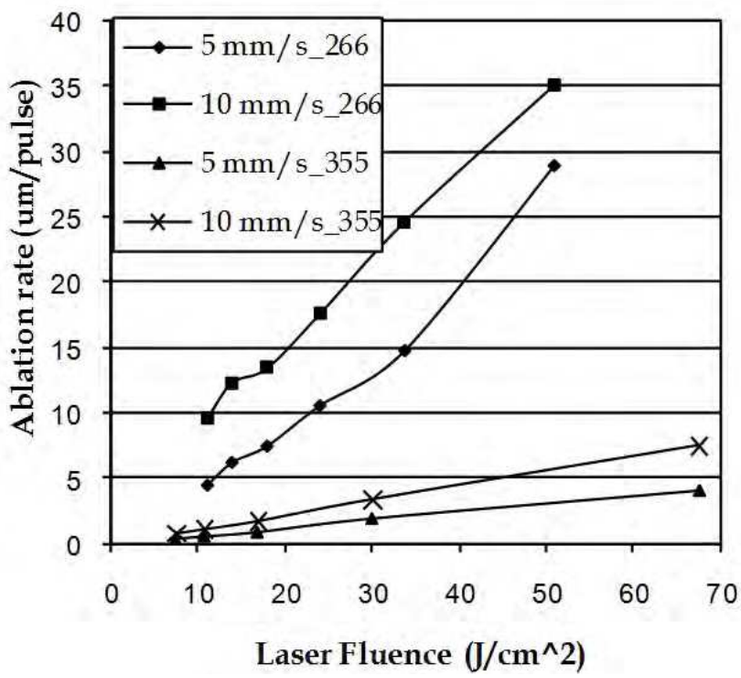

Fig. 8. The ablation rates for laser micromachining versus laser fluences for Pyrex with different cutting speeds using 266 nm and 355 nm Nd:YAG lasers.

3.3 The ablation efficiency

The ablation efficiency was calculated by dividing the ablation rate by the energy per pulse to normalize the ablation rate performed by the 355 nm and 266 nm Nd:YAG lasers. Figures 9 - 11 show the plots of ablation efficiency as a function of laser fluence with various scan speeds using both lasers. The results indicate that at high laser fluences, the ablation efficiencies of the 266 nm laser are better than that of the 355 nm laser for all three materials.

Figure 10 (silicon) shows that the ablation rate of 266 nm Nd:YAG laser micromachining is slower than 355 nm laser micromachining under 50 mm/s scan speed after normalizing the ablation rate by energy per pulse. The result points out that at the laser fluences higher than 10 J/cm^2, the ablation efficieny of the 266 nm laser is 1.5 times faster than that of the 355 nm laser at the scan speed of 50 mm/s, and 3.2 times faster in the case of 20 mm/s as shown in Table 3.

	Sapphire	Silicon		Pyrex
		50 mm/s	20 mm/s	
Ablation Efficiency 266 nm/355 nm	9	1.5	3.2	13

Table 3. The comparison of Nd:YAG 266 nm and 355 nm laser ablation efficiencies to sapphire, silicon and Pyrex with laser fluence larger than 10 J/cm^2.

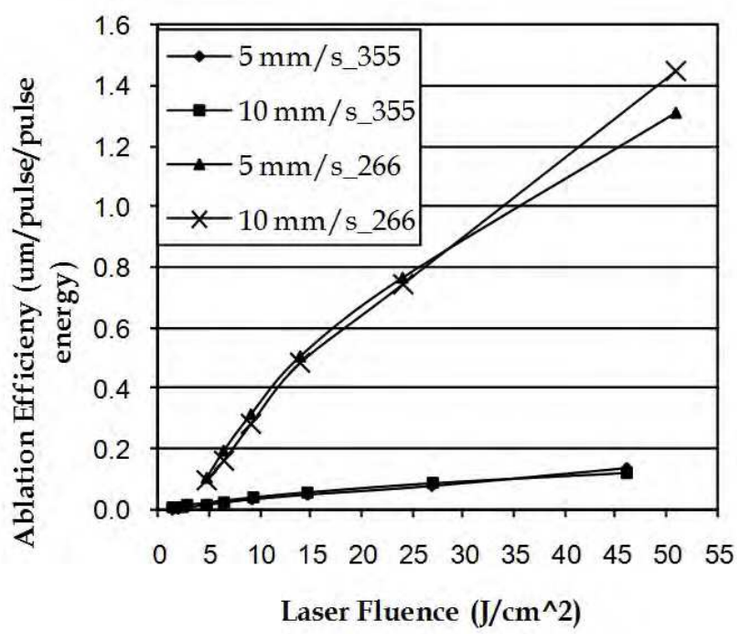

Fig. 9. Laser ablation efficiency versus laser fluences for sapphire under different scan speeds using the 266 nm and 355 nm Nd:YAG lasers.

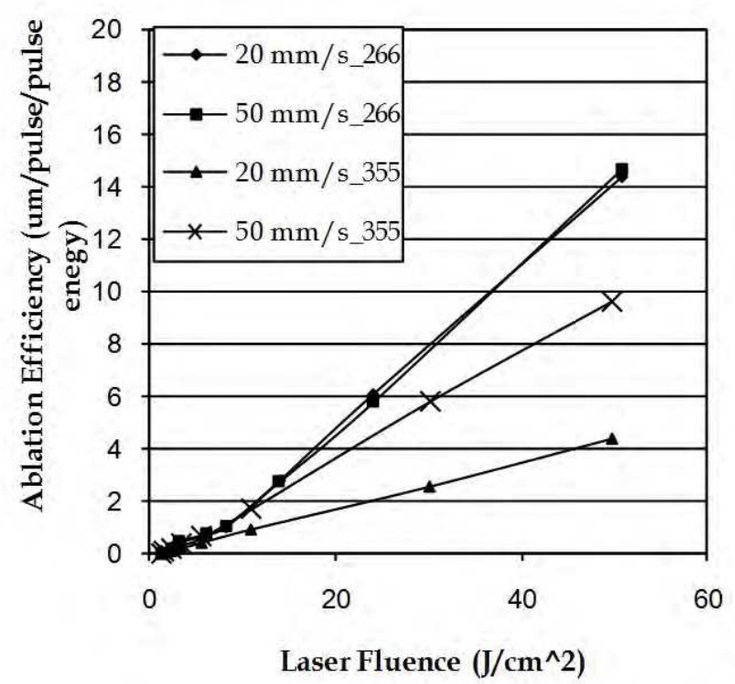

Fig. 10. Laser ablation efficiency versus laser fluence for silicon under different scan speeds using the 266 nm and 355 nm Nd:YAG lasers.

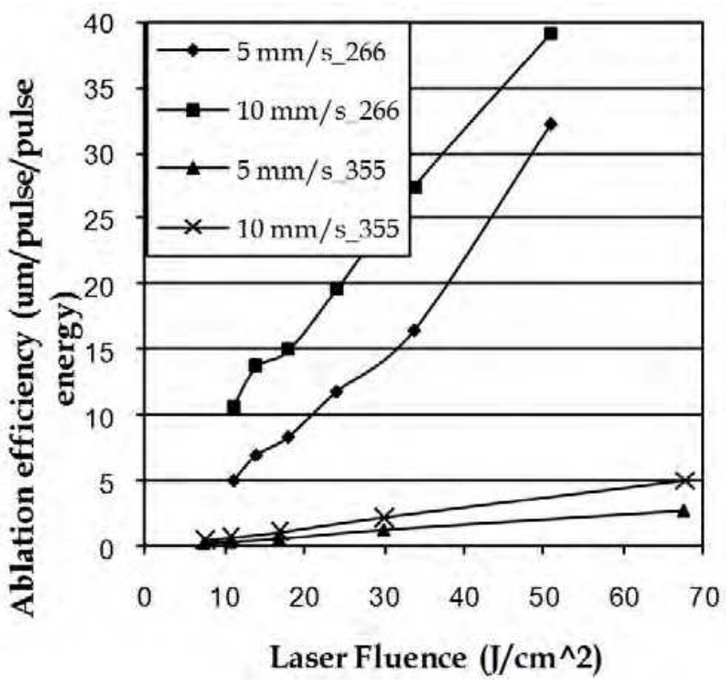

Fig. 11. Laser ablation efficiency versus laser fluence for Pyrex under different scan speeds using the 266 nm and 355 nm Nd:YAG lasers.

3.4 The ablation precision of laser micromachining

By computing the average ablation depths and standard deviation, the depth of laser micromachining can be characterized as:

Average depth (mean) ± standard error (=2.58 × standard deviation/ square root(sample size));

which give 99% of the cutting depths falling into this range (Lindgren et al., 1978), and the laser machining precision is defined as,

Precision = 2 × standard error / average depth

Figure 12 shows the plot of laser machining precision as a function of laser fluence using Nd:YAG 266 nm and 355 nm lasers with different scan speeds. The results portray the Nd:YAG 266 nm laser providing better precision than the 355 nm laser, and Nd:YAG laser micromachining more generally providing better precision in the order of sapphire, silicon and then Pyrex.

4. CO_2 laser cutting of microfluidic plastic laminates

CO_2 lasers have become the most used laser system for industrial fabrication and materials processing. This is due to a combination of their relatively low cost, high optical power and efficiency, and robust operation over a long service life. They are routinely applied to an extremely wide range of material processing, including scribing, marking, drilling, cutting, and heat treating of metals, ceramics, and polymers. CO_2 laser processing has also been

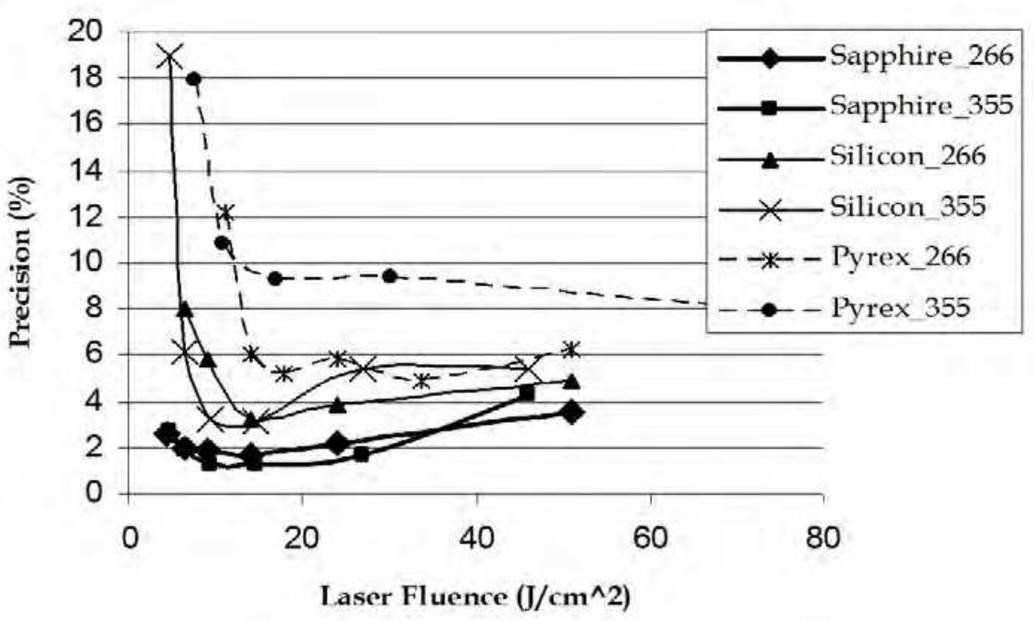

Fig. 12. Laser micromachining precision versus laser fluences for sapphire, silicon and Pyrex using the 266 nm and 355 nm Nd:YAG lasers.

extensively applied to the field of microfluidics, principally in the form of through-cutting of plastic laminates. A great many applications for microfluidics demand disposable cartridges for the liquid contacting elements of the system. Disposable cartridges, in turn, demand extremely low cost materials and fabrication methods, often in the range of pennies per part, to be competitive in the marketplace. One approach, which has gained great popularity over the past decade, is the construction of microfluidic cartridges from a series of laser-cut plastic laminates which are aligned and bonded together. This method of fabrication offers enormous flexibility in both the design of the microfluidic plumbing as well as the materials which are used to create it.

One example of a fairly advanced microfluidic cartridge created as a bonded stack of laser-cut plastic laminates is shown in Fig. 13. (Lafleur, 2010). As illustrated, this type of microfluidic cartridge can utilize both thick, rigid layers as well as thinner, flexible layers in its construction, allowing channel thicknesses from a few mils up to several mm to be created. The layers can be aligned and bonded together using a variety of techniques, including heat fusing, heat staking, solvent welding, or through the use of adhesives which are either applied directly, or which can be a pressure-sensitive adhesive which comes on one or both sides of a given layer. The cartridge shown in Fig. 13 only uses 6 layers, but cartridges employing over 20 layers are becoming more routine (Lafleur, 2010). Common structural materials for plastic laminate microfluidics include polymethyl methacrylate (PMMA), polyethylene (PE), polycarbonate (PC), and acetate. In addition, semi-permeable membranes such as Nafion and nitrocellulose are frequently employed. As is true for other types of microfluidic systems, the control of surface hydrophobicity / hydrophilicity is of paramount concern, and plays a predominant role in the materials selection.

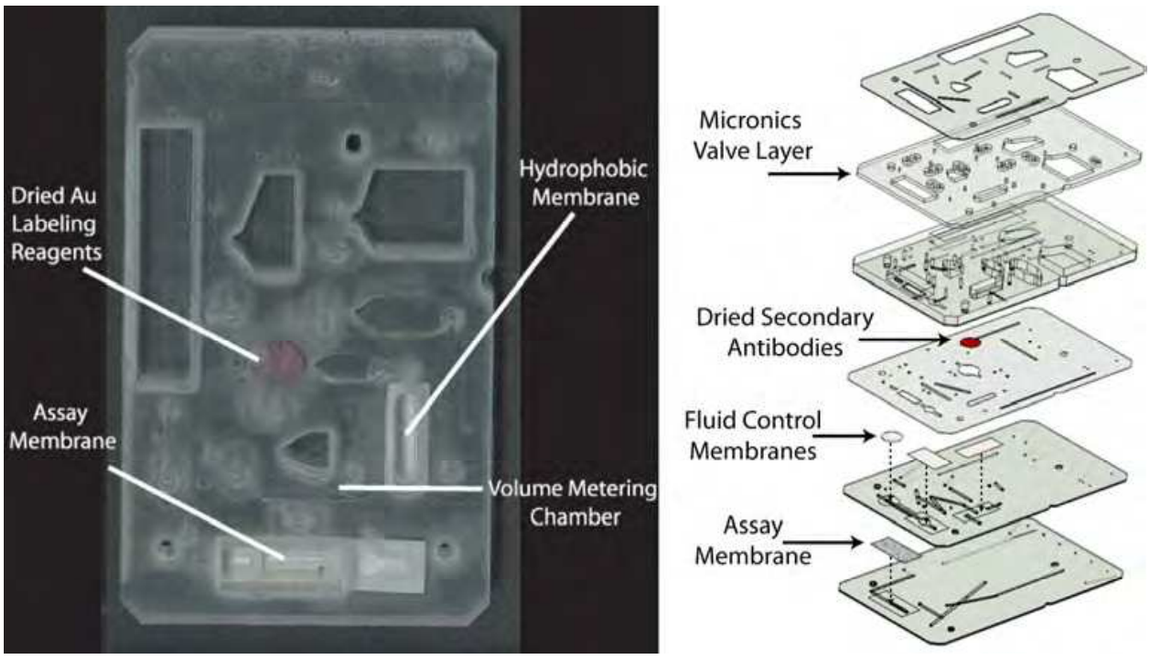

Fig. 13. A laser-cut plastic laminate microfluidic cartridge for carrying out an immunoassay. From Lafleur (2010).

5. Discussion

The laser ablation processes, thermal and photochemical, are determined by the materials properties. Figure 14 depicts the absorption coefficients of transparent materials, sapphire and Pyrex, and Table 4 shows some physical properties of those three materials.

	Eg (eV)	Melting temp. (C)	Bond strength (kJ/mol)	Absorption Coefficient@ 266nm(cm^{-1})	Absorption Coefficient@ 355nm(cm^{-1})	Evaporation Temp.* (C)
Sapphire	7.8	2054	511± 3	5.19	4.74	1800
Silicon	1.12	1414	326.8±10	2.0E6	1.07E6	1350
Pyrex	7.8	821	799.6±11.3	14.7	1.93	--

* Rough estimates of source evaporation temperatures are commonly based on the assumption that vapor pressures of 10^{-2} Torr must be established to produce efficient source removal rates (Maissel & Glang, 1970).

Table 4. Some physical properties of sapphire, silicon, and Pyrex (Chen & Darling, 2005, 2008)

In general, the laser ablation rates of sapphire, silicon, and Pyrex micromachined by near UV (355 nm) and mid-UV (266 nm) nanosecond pulsed Nd:YAG lasers, are higher using the 266 nm laser than the 355 nm laser in the absence of plume screening effects. Under those high laser fluency micromachining conditions, non-linear optical phenomena such as multi-photon process become important, and the 266 nm laser (with photon energy = 4.66 eV) has a higher probability to induce photochemical process than the 355 nm laser (with photon energy = 3.50 eV). Therefore, the ablation rates increase more in the cases of wide bandgap materials, such as sapphire and Pyrex, than the increase in the case of narrow bandgap material, like silicon as laser fluence increasing.

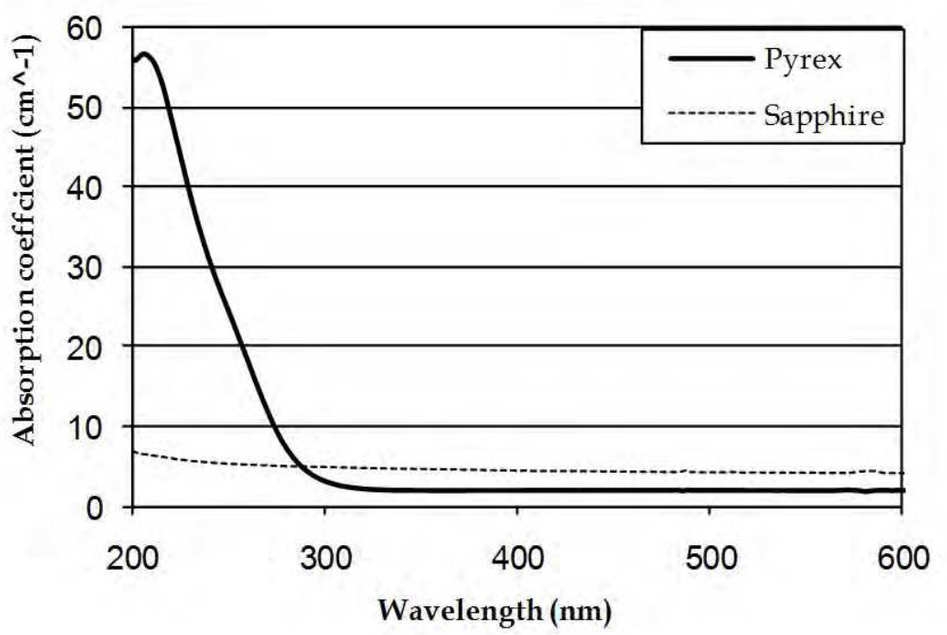

Fig. 14. The absorption coefficients versus wavelength for the transparent materials tested.

Sapphire has relatively the same level of absorption at 266 nm and 355 nm, however, the 266 nm laser provides a higher ablation efficiency at a given laser fluence than the 355 nm laser caused by higher photochemical process contributing to the overall ablation. Therefore, 266 nm laser micromachining on sapphire would provide not only slighly better absorption but also higher probability of photochemical process than 355 nm laser. In the case of silicon with its narrow band gap and high absorption at both wavelengths, the ablation efficiencies are not much different between the 266 nm and 355 nm lasers.

Pyrex has a low melting temperature, a high bond strength, a low absorption coefficient, and a wide energy band gap, as shown in Table 4. This implies that a predominantly thermal process was engaged in the laser micromachining of Pyrex by the 266 nm and 355 nm lasers. However, Pyrex shows better ablation efficiency using 266 nm laser due to more photochemical process at the higher absorption coefficient and higher energy (Mai & Nguyen, 2002; Baeuerle, 2000; Lim & Mai, 2002; Craciun & Craciun, 1999; Craciun et al., 2002; Hermanns, 2000).

Laser micromachining of plastic laminates for microfluidics nearly always involves through-cutting of each layer. CO_2 laser systems do not offer sufficient beam control to allow accurate machining to a prescribed depth, nor would the inhomogeneity of the plastic films support this type of machining. During the laser micromachining, plastic laminates are most often supported on mesh or grille working platens to allow the beam and the ablation debris to completely pass through to the other side without obstruction. Very thin, fragile or flexible materials, such as nitrocellulose membranes, are usually supported by a sacrificial backing piece, and for this situation, the laser micromachining reverts back to pure surface ablation with the debris exiting from the same side as which the laser was incident. The greatest issue with CO_2 laser through-cutting of plastics is the degree of edge melting that occurs along the kerf. While the vaporization temperatures for most plastics are comparatively low, so are the melting temperatures, and the CO_2 laser beam is both broad in diameter and deeply penetrating, all of which can combine to easily cause run-away heating of the areas surrounding the desired kerf. This is particularly a problem in CW CO_2 systems. The most common approach to combating this problem is to tune the beam traversal speed to a fairly high value which produces a shallow depth of cut, and then to scan back and forth repeatedly until the full depth of cut is achieved. The time between successive passes is chosen to be greater than the time required for the substrate to cool back down to a stable working point. Through cutting of laminates does offer the advantage that larger cavities and channels can be created by simply tracing the beam around their edges and dropping out the waste as one single piece, as opposed to scanning back and forth to ablate away the entire volume. This conserves laser beam time, minimizes heating, and creates finished parts faster, with the only negative feature being the need to reliably capture the waste pieces so that they do not get caught in the remainder of the manufacturing process.

Nearly all of the materials used for plastic laminate microfluidics can also be readily photochemical ablated by UV lasers, usually producing harmless H_2O and CO_2 gas as by products. UV laser cutting of plastics is a premier method that gives the best geometrical accuracy due to the smaller beam spot and the photochemical ablation process which produces significantly less edge melting along the kerf. However, CO_2 lasers still dominate the market for this type of machining as a result of their much lower cost and ease of use as compared to UV laser systems.

6. Conclusion

This chapter discusses the fundamentals of laser ablation in the microfabrication of microfluidic materials. The removal of material involves both thermal and chemical processes, depending upon how the laser radiation interacts with the substrate. At longer wavelengths and low laser fluencies, the thermal process dominates. While the photon energy of the laser radiation is sufficiently high, the laser radiation can provide heating, with or without melting the substrate material, and then vaporize it. At shorter wavelengths, the ablation process shifts to photochemical. The photon energy of laser radiation reaches the level of the chemical bond strength of the substrate, and then breaks these chemical bonds through direct photon absorption, leading to volatilization of the substrate into simpler compounds.

In the cases of the ablation rates of sapphire, silicon, and Pyrex, micromachined by near UV and mid-UV nanosecond pulsed Nd:YAG lasers. All three materials have higher ablation efficiencies using the 266 nm laser than the 355 nm laser due to better absorption and higher probability of photochemical process using 266 nm laser. The ablation efficiencies are increased more for the case of high melting temperature or/and finite absorption materials such as sapphire and Pyrex. The increase is less for narrow band gap or/and high absorption materials such as silicon.

Laser systems can micromachine materials all the way from lightweight plastics and elastomers up through hard, durable metals and ceramics by carefully selecting laser wavelengths, pulse duration, and fluencies. This versatility makes laser micromaching extremely attractive for prototyping and development, as well as for small to medium run manufacturing.

7. References

Ashby, M. F. & Easterling, K. E. (1984). The transformation hardening of steel surfaces by laser beams – I. Hypo-eutectoid steels. *Acta Metal.*, Vol. 32, No. 11. pp. 1935-1948, ISSN: 0001-6160

Atanasov, P. A., Eugenieva, E. D., & Nedialkov, N. N. (2001). Laser drilling of silicon nitride and alumina ceramics: A numerical and experimental study. *J. Appl. Phys.*, Vol. 89, No. 4. pp. 2013-2016, ISSN: 0021-8979

Baeuerle, D. (2000). *Laser Processing and Chemistry* (3rd Ed.), Springer, ISBN 3-540-66891-8, New York, United States of America

Bang, S. Y., Roy, S. & Modest, M. F. (1993). CW laser machining of hard ceramics–II. Effects of multiple reflections. *Int. J. Heat Mass Transfer*, Vol. 36, No. 14, pp. 3529-3540, ISSN: 0017-9310

Berrie, P. G. & Birkett, F.N. (1980). The drilling and cutting of polymethyl methacrylate (Perspex) by CO_2 laser. *Opt. Lasers Eng.*, Vol. 1, No. 2, pp. 107-129, ISSN: 0143-8166

Carslaw, H. S. & Jaeger, J. C. (1959). *Conduction of Heat in Solids* (2nd Ed.), Oxford University Press, ISBN 0-19-853303-9, Oxford, UK

Chang, J. J. & Warner, B. E. (1996). Laser-plasma interaction during visible-laser ablation of methods. *Appl. Phys. Lett.*, Vol. 69, No. 4, pp. 473-475, ISSN: 0003-6951

Chen, T.-C. & Darling, R.B. (2005). Parametric studies on pulsed near ultraviolet frequency tripled Nd:YAG laser micromachining of sapphire and silicon. *J. Mater. Sci. Technol.*, Vol. 169, No. 2, pp. 214–218. ISSN: 1005-0302

Chen, T.-C. & Darling, R.B. (2008). Laser micromachining of the materials using in microfluidics by high precision pulsed near and mid-ultraviolet Nd:YAG lasers. *J. Mat. Proc. Tech.*, Vol. 198, No. 1-3, pp. 248-253, ISSN: 0924-0136

Craciun, V. & Craciun, D. (1999). Evidence for volume boiling during laser ablation of single crystalline targets. *Appl. Surf. Sci.*, Vol. 138–139, pp. 218–223, ISSN: 0169-4332

Craciun, V., Bassim, N., Singh, R.K., Craciun, D., Hermann, J., & Boulmer-Leborgne, C. (2002). Laser-induced explosive boiling during nanosecond

laser ablation of silicon. *Appl. Surf. Sci.*, Vol. 186, No. 1-4, pp. 288–292, ISSN 0169-4332

Crane, K. C. A. & Brown, J. R. (1981). Laser-induced ablation of fibre/epoxy composites. *J. Phys. D: Appl. Phys.*, Vol. 14, No. 12, pp. 2341-2349, ISSN: 0022-3727

Crane, K. C. A. (1982). Steady-state ablation of aluminium alloys by a CO_2 laser. *J. Phys. D: Appl. Phys.*, Vol. 15, No. 10, pp. 2093-2098, ISSN: 0022-3727

Dauer, S., Ehlert, A., Buttgenbach, S. (1999). Rapid prototyping of micromechanical devices using a Q-switched Nd:YAG laser with optional frequency doubling. *Sens. Actuators A*, Vol. A76, No. 1-3, pp. 381–385, ISSN: 0924-4247

Ehrlich, D.J. & Tsao, J.Y. (Eds.). (1989). *Laser Microfabrication: Thin Film Processes and lithography*, Academic Press, ISBN-10: 0122334302 Salt Lake City, USA

Eloy, J.-F. (1987). *Power Lasers*, Halsted Press / John Wiley & Sons, ISBN 0-470-20851, New York, New York

Engin, D. & Kirby, K. W. (1996). Development of an analytical model for the laser machining of ceramic and glass-ceramic materials. *J. Appl. Phys.*, Vol. 80, No. 2. pp. 681-690, ISSN: 0021-8979

Gower, M. C. (2000). Industrial applications of laser micromachining. *Optics Express*, Vol. 7, No. 2, pp. 56-67, ISSN: 1094-4087

Hermanns, C. (2000). Laser cutting of glass, *Proc. SPIE 4102 international symposium on Inorganic Optical Materials II*, pp. 219-226, ISBN: 9780819437471, San Diego, [California], USA, August 2000

Ion, J. C., (2005). *Laser Processing of Engineering Materials*, Elsevier Butterworth-Heinemann, ISBN 0-7506-6079-1, Oxford, UK / Burlington, Massachusetts

Kaplan, A. F. H. (1996). An analytical model of metal cutting with a laser beam. *J. Appl. Phys.*, Vol. 79, No. 5, pp. 2198-2208, ISSN: 0021-8979

Knowles, M. R. H. (2000). Micro-ablation with high power pulsed copper vapor lasers. *Optics Express*, Vol. 7, No. 2, pp. 50-55, ISSN: 1094-4087

Koechner, W. (1988). *Solid-State Laser Engineering* (2nd Ed.), Springer-Verlag, ISBN 0-387-18747-2, New York, New York

Kuhn, K. J. (1998). *Laser Engineering*, Prentice Hall, ISBN 0-02-366921-7, Upper Saddle River, New Jersey

Lafleur, L. K. (2010). *Design and Testing of Pneumatically Actuated Disposable Microfluidic Devices for the DxBox: A Point-of-Care System for Multiplexed Immunoassay Detection in the Developing World*, Ph.D. Dissertation, The University of Washington, Seattle, Washington

Lash J. S. & Gilgenbach, R. M. (1993). Copper vapor laser drilling of copper, iron, and titanium foils in atmospheric pressure air and argon. *Rev. Sci. Inst.*, Vol. 64, No. 11, pp. 3308-3313, ISSN: 0034-6748

Lim, G. C., & Mai, T.-A. (2002). Laser micro-fabrications: present to future applications, *Proc. SPIE 4426 Second International Symposium on Laser Precision Microfabrication*, pp. 170-176, ISBN: 9780819441379, Singapore, May 2001

Lindgren, B.W., McElrath, G.W., Berry, D.A. (1978). *Introduction to Probability and Statistics*. (4th Ed.) Macmillan Publishing Co., ISBN: 0023709006, Basingstoke UK

Luft, A., Franz, U., Emsermann, A., Kaspar, J. (1996). A study of thermal and mechanical effects on materials induced by pulsed laser drilling. *Appl. Phys. A*, Vol. 63, No. 2, pp. 93–101. ISSN: 0947-8396

Maissel, L.I., & Glang, R. (1970). *Handbook of Thin Film Technology,* McGraw-Hill, ISBN-10: 0070397422, New York

Mai, T.-A., & Nguyen, N.-T. (2002). Fabrication of micropumps with Q-switched Nd: YAG, *Proc. SPIE 4426 Second International Symposium on Laser Precision Microfabrication*, pp. 195-202, ISBN: 9780819441379, Singapore, May 2001

Olson, R. W. & Swope, W. C. (1992). Laser drilling with focused Gaussian beams. *J. Appl. Phys.*, Vol. 72, No. 8, pp. 3686-3696, ISSN: 0021-8979

Schuöcker, D. (1999). *High Power Lasers in Production Engineering*, Imperial College Press / World Scientific, ISBN 981-02-3039-7, London / Singapore

Tunna, L., Kearns, A., O'Neill, W., & Sutcliffe, C. J. (2001). Micromachining of copper using Nd:YAG laser radiation at 1064, 532, and 355 nm wavelengths. *Optics & Laser Tech.*, Vol. 33, No. 3, pp. 135-143, ISSN: 0030-3992

Vatsya, S. R., Bordatchev, E. V. & Nikumb, S. K. (2003). Geometrical modeling of surface profile formation during laser ablation of materials. *J. Appl. Phys.*, Vol. 93, No. 12, pp. 9753-9759, ISSN: 0021-8979

Verdeyen, J. T. (1989). *Laser Electronics* (2nd Ed.), Prentice Hall, ISBN 0-13-523630-4, Englewood Cliffs, New Jersey

Voisey, K. T., Kudasia, S. S., Rodden, W. S. O., Hand, D. P., Jones, J. D. C., & Clyne, T. W. (2003). Melt ejection during laser drilling of metals. *Mat. Sci. Eng.*, Vol. A356, No. 1-2, pp. 414-424, ISSN: 0921-5093

von der Linde, D., Sokolowski-Tinten, K., & Bialkowski, J. (1997). Laser-solid interaction in the femtosecond time regime. *Appl. Surf. Sci.*, Vol. 109/110, pp. 1–10, ISSN:0169-4332.

Yuan, D. & Das, S. (2007). Experimental and theoretical analysis of direct-write laser micromachining of polymethyl methacrylate by CO_2 laser ablation. *J. Appl. Phys.*, Vol. 101, No. 2, pp. 024901-1-6, ISSN: 0021-8979

Yung, K. C., Mei, S. M., & Yue, T. M., (2002). A study of the heat-affected zone in the UV YAG laser drilling of GFRP materials. *J. Mat. Proc. Tech.*, vol. 122, pp. 278-285, ISSN: 0924-0136

Zeng, D., Latham, W. P., & Kar, A. (2005). Two-dimensional model for melting and vaporization during optical trepanning. *J. Appl. Phys.*, Vol. 97, No. 10, pp. 104912-1-7, ISSN: 0021-8979.

Zeng, D., Latham, W. P., & Kar, A. (2006). "Shaping of annular laser intensity profiles and their thermal effects for optical trepanning. *Opt. Eng.*, Vol. 45, No. 1, pp. 014301-1-9, ISSN: 0091-3286

Zhang, C., Salama, I. A., Quick, N. R., & Kar, A. (2006). One-dimensional transient analysis of volumetric heating for laser drilling. *J. Appl. Phys.*, vol. 99, No. 11, pp. 113530-1-10, ISSN: 0021-8979

Zhang, C., Quick, N. R. & Kar, A. (2008). A model for self-defocusing in laser drilling of polymeric materials. *J. Appl. Phys.*, Vol. 103, No. 1, pp. 014909-1-8, ISSN: 0021-8979

Zhou, M., Zeng, D. Y., Kan, J. P., Zhang, Y. K., Cai, L., Shen, Z. H., Zhang, X. R., & Zhang, S. Y., (2003). Finite element simulation of the film spallation process induced by the pulsed laser peening. *J. Appl. Phys.*, vol. 94, no. 5, pp. 2968-2975, ISSN: 0021-8979

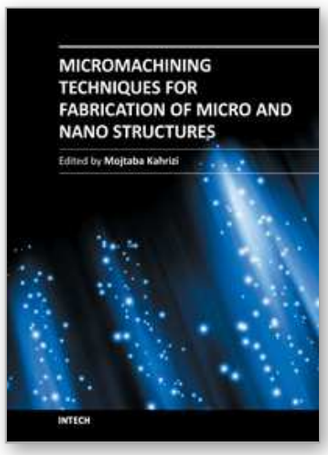

Micromachining Techniques for Fabrication of Micro and Nano Structures

Edited by Dr. Mojtaba Kahrizi

ISBN 978-953-307-906-6
Hard cover, 300 pages
Publisher InTech
Published online 03, February, 2012
Published in print edition February, 2012

Micromachining is used to fabricate three-dimensional microstructures and it is the foundation of a technology called Micro-Electro-Mechanical-Systems (MEMS). Bulk micromachining and surface micromachining are two major categories (among others) in this field. This book presents advances in micromachining technology. For this, we have gathered review articles related to various techniques and methods of micro/nano fabrications, like focused ion beams, laser ablation, and several other specialized techniques, from esteemed researchers and scientists around the world. Each chapter gives a complete description of a specific micromachining method, design, associate analytical works, experimental set-up, and the final fabricated devices, followed by many references related to this field of research available in other literature. Due to the multidisciplinary nature of this technology, the collection of articles presented here can be used by scientists and researchers in the disciplines of engineering, materials sciences, physics, and chemistry.

INTECH
open science | open minds

InTech Europe
University Campus STeP Ri
Slavka Krautzeka 83/A
51000 Rijeka, Croatia
Phone: +385 (51) 770 447
Fax: +385 (51) 686 166
www.intechopen.com

InTech China
Unit 405, Office Block, Hotel Equatorial Shanghai
No.65, Yan An Road (West), Shanghai, 200040, China
中国上海市延安西路65号上海国际贵都大饭店办公楼405单元
Phone: +86-21-62489820
Fax: +86-21-62489821

IntechOpen